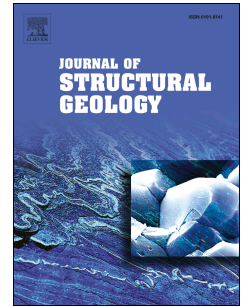


Accepted Manuscript

Tectonic strain recorded by magnetic fabrics (AMS) in plutons, including Mt Kinabalu, Borneo: A tool to explore past tectonic regimes and syn-magmatic deformation

A. Burton-Johnson, C.G. Macpherson, J.R. Muraszko, R.J. Harrison, T.A. Jordan



PII: S0191-8141(18)30433-4

DOI: <https://doi.org/10.1016/j.jsg.2018.11.014>

Reference: SG 3781

To appear in: *Journal of Structural Geology*

Received Date: 23 August 2018

Revised Date: 30 November 2018

Accepted Date: 30 November 2018

Please cite this article as: Burton-Johnson, A., Macpherson, C.G., Muraszko, J.R., Harrison, R.J., Jordan, T.A., Tectonic strain recorded by magnetic fabrics (AMS) in plutons, including Mt Kinabalu, Borneo: A tool to explore past tectonic regimes and syn-magmatic deformation, *Journal of Structural Geology* (2019), doi: <https://doi.org/10.1016/j.jsg.2018.11.014>.

This is a PDF file of an unedited manuscript that has been accepted for publication. As a service to our customers we are providing this early version of the manuscript. The manuscript will undergo copyediting, typesetting, and review of the resulting proof before it is published in its final form. Please note that during the production process errors may be discovered which could affect the content, and all legal disclaimers that apply to the journal pertain.

1 **Tectonic strain recorded by magnetic fabrics (AMS) in plutons, including**
2 **Mt Kinabalu, Borneo: A tool to explore past tectonic regimes and syn-**
3 **magmatic deformation**

4

5 Burton-Johnson, A^{a*}, Macpherson, C.G.^b, Muraszko, J.R. ^c, Harrison, R.J.^c, and
6 Jordan, T.A.^a

7

8 ^aBritish Antarctic Survey, High Cross, Madingley Road, Cambridge, CB3 0ET, UK

9 ^bDepartment of Earth Sciences, University of Durham, Durham, DH1 3LE, UK

10 ^cDepartment of Earth Sciences, University of Cambridge, Cambridge, CB2 3EQ,
11 UK

12 *Author for correspondence

13 E-mail: alerto@bas.ac.uk

14 Tel. +44 (0)1223 221284

15 Keywords: Tectonics; Magnetic fabrics; Magmatic fabrics; Intrusions; Granites;
16 SE Asia; Mt Kinabalu

17 **Highlights**

18 (1) The tectonic fabric in the AMS data of Mt Kinabalu, Borneo, reveals
19 Miocene extension in SE Asia between 7.9-7.3 Ma (later than previously
20 recognised). Correcting for paleomagnetic rotation, extension was
21 oriented NW-SE at $319^\circ \pm 13.1^\circ$.

22 (2) Tectonic strain fabrics are far more ubiquitous in global plutonic fabrics
23 than previously recognised.

24 (3) AMS determination of tectonic strain in dated plutons is a powerful tool
25 for determining past tectonics within a temporal framework, particularly
26 when combined with evidence for paleomagnetic rotation.

27 **Abstract**

28 Tectonic strain commonly overprints magmatic fabrics in AMS (Anisotropy of
29 Magnetic Susceptibility) data for plutonic rocks produced by both compressional
30 and extensional regimes. Mt Kinabalu, Borneo, is a composite pluton with an
31 exceptional vertical range of exposure and clearly defined internal contacts. We
32 show that tectonic fabrics are recorded pervasively throughout the intrusion,
33 even near contacts, and present a workflow distinguishing compressive and
34 extensional syn-magmatic deformation. At Mt Kinabalu this reveals a pervasive
35 tectonic fabric indicating NW-SE Miocene extension in Borneo at 7.9-7.3 Ma,
36 later than previously recognised, oriented NW-SE at $319^\circ \pm 13.1^\circ$. Comparing
37 data from Mt Kinabalu with data from globally distributed studies shows that
38 tectonic strain is commonly recorded by plutons. Therefore, AMS fabric can be
39 used to identify the syn-magmatic tectonic setting and combined with both
40 geochronology and evidence for paleomagnetic rotation to provide a powerful
41 tool for accurate determination of syn-magmatic tectonic regimes and strain
42 orientations within temporal frameworks.

43

44 **1. Introduction**

45 Determining syn-magmatic strain is a challenge for research into plutonic
46 intrusions because traditional structural evidence (faults and dykes) can only
47 record the post-magmatic deformation of their host pluton. Instead, evidence is
48 obtained from mineral fabric alignment (Hutton, 1988; Pitcher, 1997; Paterson
49 et al., 1998; Schofield and D'Lemos, 1998). Be this visible alignment of the rock-
50 forming phases, or more subtle alignment of the magnetically susceptible phases,
51 the recorded strain results from combined magmatic, tectonic, and lithostatic
52 stresses during crystallisation.

53 Identifying the effects of magmatic or tectonic strain provides valuable
54 information. For example, a magma flow fabric would inform how plutons are
55 intruded, whilst a tectonic fabric would record the tectonic strain orientation
56 during emplacement. However, contrasting interpretations of plutonic mineral
57 fabrics as the recorders of magmatic flow or tectonic strain exist, even for similar
58 intrusions and tectonic settings (e.g. Petronis and O'Driscoll, 2013; Tomek et al.,
59 2016).

60 In this study we use field and magnetic fabric (AMS, Anisotropy of Magnetic
61 Susceptibility) data from the Mt Kinabalu intrusion of Borneo to demonstrate the
62 pervasive overprint of tectonic fabrics upon magmatic fabrics.. We use the Mt
63 Kinabalu intrusion to demonstrate that determining these tectonic fabrics by
64 AMS offers a powerful tool to obtain temporal constraints on past tectonic
65 regimes. In this case, we constrain the syn-magmatic deformation during a
66 period of disputed tectonics in SE Asia. We compare this with data from other
67 globally distributed plutons to show that such records of deformation are
68 commonly present in granitic plutons,

69 **2. Application of AMS to mineral fabric research**

70 Mineral fabrics in granitic plutons have long been mapped and studied but
71 accurate determinations of these fabrics are often difficult and observations risk
72 being biased by the two dimensional nature of an outcrop. Consequently,
73 analysis of the Anisotropy of Magnetic Susceptibility (AMS) has frequently been
74 applied to granitic intrusions (Bouchez, 1997). This method measures variation

75 in the susceptibility of each of the three, principal, magnetic axes of an oriented
76 sample (Jezek and Hrouda, 2004); K1, the axis of maximum magnetic
77 susceptibility; K3, the axis of minimum susceptibility; and K2, the intermediate
78 axis (Fig. 1). This method allows fast, inexpensive, and accurate determination of
79 three-dimensional mineral fabrics even when such fabric cannot be observed in
80 outcrop.

81 Magnetic fabrics can be hosted by ferro-, ferri-, para-, or diamagnetic phases.
82 These classifications and the grain size of the carrier phase determine the nature
83 of observed magnetic fabrics. The magnetic susceptibility of ferro- and
84 ferrimagnetic phases (e.g. magnetite, and pyrrhotite) is three orders of
85 magnitude greater than paramagnetic phases (Hunt et al., 1995). In
86 ferromagnetic minerals all magnetic moments align, whilst in ferrimagnetic
87 minerals some point in the opposite direction. Below their Curie temperature,
88 ferro- and ferrimagnetic phases magnetise when exposed to a magnetic field and
89 remain magnetic once the field is removed. In contrast, the much less magnetic
90 phases exhibiting paramagnetism (e.g. biotite and hornblende) cease being
91 magnetic once the field is removed. The weakest magnetic effect occurs in
92 diamagnetic minerals (e.g. quartz), which are often classed as 'non-magnetic'.

93 Magnetic domains in ferro- and ferrimagnetic phases cause their magnetic
94 susceptibility to be grain size dependent, with larger grains displaying greater
95 susceptibilities (Hunt et al., 1995). As grain size increases the magnetic domain
96 state changes from single-domain to multi-domain. This is important for AMS
97 studies, as whilst the axes of magnetic susceptibility in multi-domain grains (and
98 the paramagnetic phases biotite and amphibole; Bouchez, 1997) correspond
99 with the grain shape, in single-domain grains the magnetic susceptibility axes
100 are inverted (Stephenson et al., 1986), producing inverse magnetic fabrics
101 (Hrouda and Jezek, 2017). Multi- and single-domain grains can be differentiated
102 by varying the temperature and magnetic field imposed on a sample, as in this
103 study.

104 3. Development of plutonic mineral fabrics

105 Magmatic mineral fabrics form during crystallisation in response to the stress
106 experienced by partially molten magma until it cools to its solidus. This stress
107 can be a result of: (1) the primary magma flow during emplacement, including
108 stress applied by the ascending magma column on the melt (e.g. Horsman et al.,
109 2005, Stevenson et al., 2006, Stevenson et al., 2007a, Clemens and Benn, 2010);
110 (2) regional tectonic stress during emplacement and crystallisation (e.g.
111 Vigneresse, 1995, Benn et al., 1997, Benn, 2009); or (3) a combination of both
112 (e.g. Wennerström and Airo, 1998, Petronis et al., 2012). Whether a plutonic
113 mineral fabric (including AMS) records magmatic or tectonic stresses will be
114 determined by the dominating force during final crystallisation of the pluton at
115 the end of its emplacement.

116 In response to syn-magmatic stress, crystals align their longest principal axis
117 with the long axis of the resultant strain ellipsoid and their shortest principal
118 axis parallel to the short axis of the strain ellipsoid (Fig. 1, Paterson et al., 1998).
119 This relationship of mineral fabric to the strain ellipsoid has been shown by
120 numerical and analogue experiments for simple, non-coaxial shear, for pure,
121 coaxial shear, and for mixed strain conditions (Jeffery, 1922; N. C. Gay, 1968; No
122 C. Gay, 1968; Arbaret et al., 1997; Schulmann et al., 1997; Schulmann and Ježek,
123 2012).

124 The relationship between stress and strain is complex and requires
125 consideration, as observed magmatic fabrics may record a spectrum from coaxial
126 to non-coaxial deformation. The resultant AMS fabrics expected for different
127 deformation settings are shown in Fig. 2. Coaxial, non-rotational shear can be
128 expected away from rheological contrasts (i.e. away from internal and external
129 contacts), resulting from tectonic stress, and stress exerted by the upwelling
130 magma and overburden (Paterson et al., 1998).

131 Under coaxial, non-rotational shear, the shortest principle axis of the strain
132 ellipsoid is parallel to the direction of maximum compressive stress (σ_1 , Fig. 1
133 and Fig. 2) whilst the longest principle axis of the strain ellipsoid will be parallel
134 to the direction of minimum compressive stress (σ_3 , Fig. 1 and Fig. 2). The degree
135 to which rigid particles (i.e. the crystal fabric) rotate in response to the strain

136 ellipsoid will increase at higher degrees of strain (N. C. Gay, 1968), increasing the
137 anisotropy of the fabric. However, assuming a random initial particle
138 distribution, even at low degrees of strain the overall distribution of the
139 respective stress and strain axes (and consequently the AMS fabric) will be
140 parallel; albeit with a lower degree of anisotropy (Arbaret et al., 2000).

141 Non-coaxial simple, transpressional, and trans-tensional shearing can be
142 expected to affect both magmatic and tectonic fabrics, particularly where there is
143 differential movement near rheological contrasts. This includes both internal and
144 external contacts (Blumenfeld and Bouchez, 1988; Paterson et al., 1998) or
145 where a pluton is emplaced along a shear zone (Archanjo et al., 1999, 2002).

146 Under non-coaxial shear, with increasing degrees of strain the longest principle
147 axis of the strain ellipsoid (and consequently the crystals) will rotate towards the
148 direction of shearing and consequent stretching (elongation) direction (Fig. 2).
149 The shortest principle axis of the strain ellipsoid and crystals will rotate towards
150 perpendicular to the rheological boundary and orthogonally to the direction of
151 extension (Fig. 2, Arbaret et al., 1997; Benn, 2010). In non-coaxial shear, the
152 relationship between stress and strain orientations is dependent on a number of
153 factors including tectonic setting, the degree of shearing, rheological contrasts
154 and pre-existing structures.

155 As noted, a crystallising melt will experience a spectrum from coaxial to non-
156 coaxial shearing, complicating derivation of stress and strain vectors. However,
157 coaxial and non-coaxial shear produce distinct and different fabrics (Fig. 2). By
158 predicting these fabrics for the magmatic and tectonic strain regimes of a pluton
159 (Fig. 2) and comparing them with the pluton's observed magmatic fabric, the
160 relative contributions of coaxial and non-coaxial shear can be determined.

161 **4. The Mt Kinabalu Intrusion, Borneo**

162 The Mt Kinabalu intrusion of Sabah, Borneo (Fig. 3), provides an ideal field area
163 to investigate magnetic mineral fabrics in three dimensions across a single
164 composite pluton. This is because it has an extensive, glaciated summit; a 2900m
165 vertical range of granitic exposure; clearly mapped internal and external
166 contacts; and strong temporal constraints on the emplacement historyThe

167 pluton intruded into the shallow crust (3-12 km, Vogt and Flower, 1989; Cottam
168 et al., 2013; Burton-Johnson et al., 2017) as six major granitic units between 7.85
169 and 7.55 Ma (Cottam et al., 2010) at the contact between the Mesozoic ophiolitic
170 ultramafic basement (Reinhard and Wenk, 1951; Dhonau and Hutchison, 1965;
171 Koopmans, 1967; Kirk, 1968; Leong, 1974) and overlying Eocene to Lower
172 Miocene turbiditic sandstones of the Crocker Formation (Collenette, 1965; van
173 Hattum et al., 2006). Contrasting geodynamic settings have been proposed for
174 NW Borneo at this time, either as a zone of regional compression (Hutchison,
175 2000; Swauger et al., 2000; King et al., 2010; Pubellier and Morley, 2013) or
176 regional extension (Cottam et al., 2013; Hall, 2013; Burton-Johnson et al., 2017).
177 Contact metamorphism of the adjacent ultramafic rocks generated talc and
178 anthophyllite, indicative of granitoid emplacement at 630-700°C and 2-3 kbar
179 (7-11 km, Bucher and Grapes, 2011).

180 Recent work (Cottam et al., 2010; Burton-Johnson et al., 2017) has shown that
181 the composite pluton was initially emplaced from the top down in a broadly
182 laccolithic structure (Fig. 3C) through upward deformation of the host rocks.
183 Consequently, the oldest unit (the Alexandra Tonalite/Granodiorite, 7.85 ± 0.08
184 Ma) overlies the subsequent, larger units (the Low's Granite, 7.69 ± 0.07 Ma, and
185 the King Granite, 7.46 ± 0.08 Ma). The smaller, vertical planar Donkey Granite
186 (7.49 ± 0.03 Ma) intruded the King Granite before the latter could fully crystallise,
187 producing contacts that vary from gradational to mingled. The final two
188 porphyritic units (the Paka Porphyritic Granite, 7.32 ± 0.09 Ma, and the Mesilau
189 Porphyritic Granite, 7.22 ± 0.07 Ma) deviate from the laccolith model having been
190 emplaced laterally and around the periphery of earlier units (Fig. 3c).

191 Mineralogies of the units are summarised in Table 1. Petrographically the units
192 are largely classified as granites (Burton-Johnson et al., 2017), although their
193 major element composition is largely granodiorite (Burton-Johnson et al., in
194 review). Hornblende is the dominant mafic phase in all units except the
195 Alexandra Tonalite/Granodiorite, in which biotite dominates. Visible mineral
196 macrofabrics are absent in all units except the Alexandra unit, in which a biotite
197 foliation was observed, dipping $\sim 40-60^\circ$ towards the south-west (Burton-
198 Johnson et al., 2017). To test this observation, image analysis (adapting the

199 methodology of Grove and Jerram, 2011) was conducted on thin sections of each
200 unit (Fig. 4), characterising the colour palettes for biotite and hornblende in each
201 section to determine the 2D orientation of the ferromagnesian crystals (Fig. 4).
202 The standardised resultant vector length, \bar{R} , (the data distribution parameter in
203 circular directional statistics, Davis 1986) is higher (i.e. more consistently
204 distributed) for the Alexandra unit than the later units for both hornblende
205 (0.008 compared to 0.002) and biotite (0.004 compared to 0.002). Furthermore,
206 no microstructural evidence for shearing was observed in the thin sections of
207 any unit (Fig. 4).

208 5. Methodology

209 Whilst the glaciated summit of Mt Kinabalu provides complete exposure, and the
210 topography provides an exceptional vertical range of outcrop, steep cliffs and
211 rainforest-covered flanks limit the area that can be sampled. However, previous
212 work has shown the remarkable lateral homogeneity of AMS fabrics in plutons at
213 a range of scales, with variations in fabric orientations occurring around a mean
214 vector (Bouchez, 1997; Olivier et al., 1997). What is less constrained is the
215 degree AMS fabric heterogeneity vertically through a pluton. The 2900m vertical
216 range of outcrop at Mt Kinabalu provides a unique opportunity to explore this,
217 and consequently sampling focussed on transects to the North, South, East and
218 West of the pluton. Samples were collected at 50m vertical intervals on the
219 summit and the accessible southern flank, and at 100m vertical intervals
220 elsewhere.

221 94 oriented block samples were collected (Fig. 5) from which 10 to 24 cylindrical
222 cores of 11cm³ were drilled per sample at the University of Birmingham, UK
223 (Owens, 1994) The number of cores depended on each sample's weathering and
224 alteration. Oriented cores were analysed on an AGICO KLY-3s Kappabridge at the
225 University of Birmingham to determine the orientation and magnitude (K) of the
226 three principal axes of the AMS fabric (K1, K2 and K3; Fig. 1). Each sub-
227 specimen's results were normalised by the specimen's mean susceptibility
228 (K_{mean}) and averaged for each block sample to determine mean values of the AMS
229 ellipsoid (Jelínek, 1978, Owens, 2000). To determine the magnetic mineralogy,

230 variability of magnetic susceptibility with temperature was determined on
231 powdered samples at the University of Cambridge, UK. An AGICO MFK1
232 Kappabridge with a CS4 high temperature attachment and CS-L low temperature
233 attachment was used under an argon atmosphere to reduce secondary oxidation.
234 Samples representing each plutonic unit were selected for detailed magnetic
235 characterisation. Hysteresis loops, DC demagnetisation curves and first-order
236 reversal curve (FORC) diagrams were collected using a Lakeshore Vibrating
237 Sample Magnetometer at the University of Cambridge.

238 **6. Results**

239 **6.1. Shape of the AMS fabric**

240 Full results are given in the supplementary material. The shape of the observed
241 AMS fabric is described according to the relative dimensions of the three
242 principal axes of the AMS ellipsoid (Fig. 1). All analysed fabrics lie along a
243 spectrum from purely oblate (a flattened spheroid where $K1 = K2 > K3$) to purely
244 prolate (an elongated spheroid where $K1 > K2 = K3$) and are described by the
245 shape parameter, T (Jelinek, 1981) which has a possible range from 1 (purely
246 oblate) to -1 (purely prolate). The degree of measured anisotropy (P' , Jelinek,
247 1981) is used instead of $K1/K3$ as it refers to deviation of all axes (including $K2$)
248 from the mean susceptibility. The bulk magnetic susceptibility (K_{Mean}) varies by
249 two orders of magnitude (Fig. 6). The mineral fabric (T) is dominantly oblate
250 (Fig. 6), but for almost all samples the axes are statistically distinct from each
251 other at 95% confidence; allowing statistically valid utilisation of all three axes
252 (including the lineation, $K1$).

253 **6.2. Magnetic mineralogy**

254 The magnetically susceptible mineralogy can be determined from the variations
255 of magnetic susceptibility with temperature (Fig. 7), hysteresis loops (Fig. 8) and
256 First Order Reversal Curves (FORC diagrams, Fig. 8). All samples except the
257 Alexandra Tonalite/Granodiorite show abrupt reductions in bulk susceptibility
258 on heating between 565-585°C, the Curie temperature of pure magnetite.
259 Although a small Hopkinson peak prior to the 565-585°C reduction in magnetic
260 susceptibility appears to be present in some samples (Fig. 7), the lack of an

261 extreme peak indicates dominance of multi-domain rather than single or pseudo
262 single-domain particles (Orlický, 1990). The susceptibility decrease at 320-
263 420°C results from the conversion of maghemitised magnetite to hematite
264 (Orlický, 1990), an interpretation supported by the absence of this feature in the
265 cooling curves. For all samples the cooling curve has a higher susceptibility than
266 the heating curve, indicating production of secondary magnetite during heating.

267 The low bulk susceptibility of the Alexandra Tonalite/Granodiorite indicates a
268 paramagnetic carrier phase, most probably biotite and/or amphibole, given the
269 mineralogy of this unit (Burton-Johnson et al., 2017). This is consistent with the
270 parabolic decrease in susceptibility at low temperature (Fig. 7) with no increase
271 at -148°C (the Verwey transition; Walz 2002), indicating that magnetite is not
272 the dominant carrier. The hysteresis loops have a high contribution from
273 paramagnetic minerals, which were corrected for in the analysis (Fig. 8). The
274 samples have low coercivity values in the range of 2.7-8.5 mT, consistent for
275 multi-domain grains (see supplementary material for full results). FORC
276 diagrams for the Alexandra Tonalite/Granodiorite and King Granite (Fig. 8) show
277 low coercivity (B_c) and a wide range in the bias field (B_u), with a weakly
278 expressed negative bias region present on the right hand side of the lobe. These
279 features all indicate multi-domain behaviour, as even small proportions of
280 single-domain grains produce the high coercivity and narrow bias range
281 associated with single-domain behaviour (Fig. 8; Harrison et al., 2018). As the
282 magnetic fabric is and hosted by multi-domain magnetite, biotite, and amphibole,
283 the AMS data does not represent an inverse fabric (as would be produced by
284 single-domain magnetite; Stephenson et al., 1986).

285 **6.3. AMS fabric of the different units**

286 Overall the fabrics of most Mt Kinabalu granitic units display lineation with a
287 shallow, NW plunge (K1; Fig. 9), and shallow dipping foliation (to which K3 is the
288 pole; Fig. 8), although there are deviations. In the Alexandra
289 Tonalite/Granodiorite, lineation of the AMS fabric (K1) shows a shallow plunge
290 to the NW whilst the foliation (K3) has a consistent moderate dip to the SW (Fig.
291 9). Lineation of the Low's Granite also plunges to the NW but the foliation dip is
292 shallower than the Alexandra unit (Fig. 9). The most sampled unit, the King

293 Granite, has the most homogenous AMS fabric with a lineation consistently
294 plunging sub-horizontally to the NW/SE and a foliation recording a very shallow
295 SW dip (Fig. 9). The Donkey Granite has the lowest areal extent and thus the
296 fewest samples. Its lineation is variable and dominantly contact-parallel (Fig. 9)
297 while the foliation has a shallow west dip (Fig. 9), although it frequently strikes
298 sub-parallel to the contacts (Fig. 5). The AMS fabric of the Paka Porphyritic
299 Granite again has a shallow NW plunge to its lineation and a shallow west dip to
300 its foliation (Fig. 9). However, deviations in both the lineation and foliation are
301 evident at the eastern extent and near internal contacts (Fig. 5). We obtained
302 relatively few measurements of the Mesilau Porphyritic Granite due to the poor
303 accessibility of the lower forested flanks of Mt Kinabalu. AMS measurements of
304 Mesilau are highly variable in both foliation and lineation (Fig. 9). Thin section
305 examinations of this unit reveal accumulations of secondary hydrothermal
306 magnetite within its fractures and along grain boundaries, leading to the poorly
307 defined AMS fabric (Fig. 9) and largest range of bulk susceptibility (Fig. 6).

308 **7. Discussion**

309 **7.1. Tectonic or magmatic fabric?**

310 The AMS fabric of Mt Kinabalu shows clear and consistent orientations through
311 most units but to understand the origin of this fabric we must determine if it
312 represents magmatic or tectonic strain. This distinction is achieved by
313 comparing the AMS fabric with field evidence for tectonic strain (Paterson et al.,
314 1998). Burton-Johnson et al. (2017) investigated the orientations and
315 relationship of several, early, post-magmatic strain indicators in and around Mt.
316 Kinabalu, including orientations of faults, aplite dykes and mafic dykes within
317 the pluton. These indicate a post-magmatic sub-vertical principal compressive
318 stress, σ_1 (i.e. lithostatic pressure), whilst the minimum compressive stress, σ_3 ,
319 was sub-horizontally NNW-SSE oriented (Fig. 10). This extensional regime
320 contrasts with the NW-SE to N-S striking compressive folds and associated thrust
321 faults of the local sedimentary country rocks (Jacobson, 1970; Burton-Johnson et
322 al., 2017), which record the Early Miocene Sabah Orogeny (Hutchison, 1996) that
323 pre-dates the intrusion.

324 Under coaxial shear, the extensional stress field recorded by the faults and dykes
325 of the pluton (Fig. 10) would be predicted to generate AMS fabrics with shallow
326 NNW-SSE plunging lineations (K1) and sub-vertically dipping poles to the
327 foliations (K3); similar to Fig. 2c. Fig. 10 shows that this is precisely the syn-
328 magmatic AMS fabric demonstrated by all units except the Donkey Granite and
329 the Mesilau Porphyritic Granite (a result of secondary magnetite), indicating
330 similar syn- and post-magmatic stress regimes. The similarity in the predicted
331 directions of extension from both the field and AMS evidence requires agreement
332 between the principal stress and strain vectors, indicating the dominance of
333 coaxial, non-rotational shear rather than non-coaxial simple shear in the
334 development of the AMS fabric (Fig. 2).

335 As discussed above, the crystallisation of secondary magnetite in the Mesilau
336 Porphyritic Granite has compromised its magnetic record. The foliation of the
337 Donkey Granite shows shallow dips (Fig. 9), however its lineations tend towards
338 contact-parallel orientations rather than the expected fabric. This orientation of
339 contact-parallel lineation and shallow foliation is generated in dykes through
340 post-flow compaction of a contact-parallel magmatic fabric (Park et al., 1988;
341 Ernst and Baragar, 1992), indicating that the deviation of the Donkey Granite
342 fabric from the overall distribution results from the narrow width of this unit
343 (Burton-Johnson et al., 2017).

344 **7.2. Effect of contacts on tectonic AMS fabrics**

345 The mechanical contrast along internal or external contacts will generate
346 contact-parallel fabrics in plutons. Simple shear elongation of the fabric will
347 occur in the stretching direction (Fig. 2d, Paterson and Tobisch, 1988; Paterson
348 et al., 1998). We have noted this effect in the narrow Donkey Granite but how far
349 from a contact does this affect AMS fabric in the larger units?

350 The contact between the King Granite and the later Paka Porphyritic Granite can
351 be traced for over 2km on the south flank of Mt Kinabalu (Fig. 5). Samples from
352 either side of the contact show that the lineation in both units reflects the
353 tectonic overprint even from samples <5m from the contact (Fig. 5c). The
354 foliation is more sensitive to contact-parallel fabrics, with the strike of samples

355 close to the boundary rotated towards the contact but only for samples up to
356 100m from the contact (Fig. 5d). The presence of a contact-parallel foliation but a
357 tectonic fabric in the lineation indicates rotation about a lineation-parallel zone
358 axis or the development of a variably contact-parallel fabric, subsequently
359 overprinted by invariable extension in the lineation direction.

360 As observed in studies of other intrusions (Bouchez, 1997; Olivier et al., 1997),
361 the AMS fabric of Mt Kinabalu shows remarkable lateral homogeneity across the
362 pluton. The vertical range of exposure at Mt Kinabalu also reveals comparable
363 vertical homogeneity. Overprinting of magmatic fabrics by tectonic strain from
364 coaxial, non-rotational shear is pervasive, even <5m from the contacts and
365 across the entire 2900m vertical range of the intrusion. This implies that
366 plutonic AMS fabrics can be used to determine syn-magmatic tectonic strain
367 even when the geometry of the pluton is unknown.

368 **7.3. Application of the AMS fabric to tectonic interpretation**

369 Excluding the two units for which the tectonic fabric is not recorded (The
370 Donkey Granite and Mesilau Porphyritic Granite), the orientations of the
371 maximum (σ_1) and minimum (σ_3) syn-magmatic tectonic compression directions
372 interpreted from AMS are in close agreement with the field evidence (Fig. 10).
373 However, unlike the syn-magmatic strain recorded by the AMS fabric, because
374 faults and dykes must postdate their host they can only date post-magmatic
375 deformation. The AMS data is also less dispersed, and less ambiguous as its
376 vectors correspond with specific vectors of the strain ellipsoid. As the AMS fabric
377 is hosted by the rock itself, it can be dated directly (unlike most faults and other
378 evidence for paleostrain) allowing determination of the strain ellipsoid at a
379 specific time. This provides a powerful tool for structural and tectonic research.

380 The paleomagnetic rotation of the Mt Kinabalu intrusions since emplacement
381 was determined from granitic samples as 11° anticlockwise ($\pm 2.4^\circ$ at 95%
382 confidence, (Fuller et al., 1991). By correcting the azimuth of the lineation
383 (eigenvector of $308^\circ \pm 10.7^\circ$ at 95% confidence, the proxy for the syn-magmatic
384 extension direction) by the paleomagnetic rotation we can determine that at 7.9-
385 7.3 Ma Sabah was undergoing NW-SE crustal extension at $319^\circ \pm 13.1^\circ$. This

386 supports the presence of a NW-SE oriented extensional regime in Sabah during
387 the Miocene, which may be the result of SE-directed slab rollback during
388 subduction of the Celebes Sea to the SE (Cottam et al., 2013; Hall, 2013). Our
389 findings are not compatible with models invoking contemporaneous tectonic
390 compression in the region (Hutchison, 2000; Swauger et al., 2000; King et al.,
391 2010; Pubellier and Morley, 2013). Emplacement during regional extension is
392 more consistent with a setting affected by slab rollback, which has been
393 proposed between 11-10 Ma (Hall, 2013), although our observations suggest
394 that extension persistent until, at least, 7.5Ma..

395 **7.4. Tectonic overprinting of magmatic AMS fabrics: A widespread** 396 **phenomenon?**

397 We have shown that extensional tectonics pervasively overprinted the AMS
398 fabric of the Mt Kinabalu intrusion. Where observed elsewhere, similar
399 observations have been utilised to infer local strain partitioning (Archanjo et al.,
400 1992, 2002; Benn, 2010), but can AMS be applied to determine tectonic
401 deformation on a global scale? To investigate whether similar overprinting
402 occurs elsewhere we compiled data from intrusions of varying age and
403 dimensions, and from globally distributed compressional and extensional
404 tectonic regimes (Fig. 11). Whilst not a complete global dataset, this provides a
405 global distribution of plutons from known tectonic settings for which there is
406 comprehensive sample coverage, and includes numerous well-recognised
407 studies (e.g. Mt Stuart, Monte Capanne, Dinkey Creek, and Mono Creek –
408 respectively (Bouillin et al., 1993; de Saint Blanquat and Tikoff, 1997; Cruden,
409 1999; Benn et al., 2001).. The tectonic settings and orientations of compression
410 or extension are from the literature, with the specific orientation shown in Fig.
411 11 determined by ourselves as in Fig. 1.

412 Some of the AMS datasets included in our compilation have already been
413 interpreted as recording a tectonic overprint (e.g. the Shellenbarger and Mt
414 Stuart plutons, USA) whilst others have not (e.g. the Pinto Peak intrusion, USA,
415 and the Monte Capanne intrusion, Italy). However, in all cases a clear and
416 consistent fabric is shown by each intrusion. For each example included in our
417 study the orientation of tectonic strain required to generate each fabric through

418 coaxial shear (as illustrated in Fig. 2) is always in agreement with the
419 contemporaneous tectonic regime of the region (Fig. 11).

420 As with Mt Kinabalu, the close agreement of the AMS fabric vectors and regional
421 tectonic stress directions in both compressional and extensional settings
422 indicates the dominance of coaxial, non-rotational shear rather than simple, non-
423 coaxial shear in pluton-scale AMS fabrics. This allows simple interpretation of
424 the stress and strain vectors. Even in plutons associated with major shear zones,
425 field studies have shown that simple shear is only pervasive close to the shear
426 zone (Gleizes et al., 2001; Tikoff et al., 2005; Benn, 2010), returning to more
427 homogenous, coaxial, non-rotational shear fabrics at greater distances from the
428 shear zone; as observed near the contacts of Mt Kinabalu. The pervasiveness of
429 the simple shear regime is dependent on the rheology of the lithology, timing and
430 degree of shearing, and the scale-dependant cooling history of the pluton
431 (Archanjo et al., 2002; Tikoff et al., 2005; Benn, 2010). Where intrusions were
432 metamorphosed and recrystallised in the deeper crust after emplacement, this
433 coaxial tectonic fabric can be imparted millions of years after magmatism
434 (Hrouda et al., 1988; Hrouda and Faryad, 2017).

435 In extensional plutons the lineation direction (K1) is consistently parallel to the
436 azimuth of extension, whilst the foliation dip varies, similar to our observations
437 in the Alexandra Tonalite/Granodiorite of Mt Kinabalu. Similarly, in
438 compressional plutons the pole to foliation (K3) is consistently in the direction of
439 compression whilst the plunge of the lineation varies. In a compressive regime
440 this lineation variation reflects whether σ_2 (Fig. 1) represents lithostatic
441 (vertical) or lateral (tectonic) compression. If σ_2 represents lithostatic
442 compression the lineation will be sub-horizontal but if the degree of tectonic
443 compression is increased and σ_2 becomes horizontal then the lineation will be
444 sub-vertical (Fig. 2a and 2b). Similarly, in an extensional regime the foliation
445 variation reflects the orientation of σ_1 (Fig. 1). If σ_1 represents lithostatic
446 compression the foliation will be sub-horizontal but if the degree of lateral
447 compression increases, and σ_1 becomes horizontal then the foliation dip will be
448 sub-vertical.

449 Because of these variations in extensional foliation and compressional lineation,
450 comparing the confidence limits of the mean K1 and K3 vectors (Fig. 12)
451 distinguishes whether a pluton was emplaced in a compressive or extensional
452 setting even in the absence of other data (e.g. field evidence for deformation).
453 Using symmetrical 95% confidence angles for the mean spherical vectors of K1
454 and K3, compressional plutons can be identified at 90% confidence where “K1
455 confidence angle / K3 confidence angle” < 1.2 , and extensional plutons can be
456 identified at 90% confidence where “K1 confidence angle / K3 confidence angle”
457 > 1.5 (Fig. 12).

458 We conclude that coaxial tectonic strain is commonly preserved in the AMS
459 fabric of plutonic intrusions. This explains the remarkable homogeneity of AMS
460 fabrics within many individual plutons (Bouchez, 1997; Olivier et al., 1997) and
461 opens up the possibility of using AMS fabrics to determine syn-magmatic
462 deformation. As intrusive magmatism is a common feature of many tectonic
463 settings throughout Earth’s history, the nature of a tectonic regime can be
464 investigated from its accompanying plutons. Just like traditional structural
465 evidence, granitic magmatism has long been seen as a product of tectonic
466 deformation (Vigneresse, 1999). By applying this technique, plutons can be used
467 as a potent structural tool for investigating those tectonic processes and
468 identifying tectonic regimes.

469 **8. Conclusions**

470 - The AMS fabric of the Mt Kinabalu intrusion, Borneo, was largely derived by
471 syn-magmatic crustal extension.

472 - Tectonic strain is highly pervasive throughout the Mt Kinabalu pluton,
473 dominating the AMS foliation to within 100m of contact surfaces, and the AMS
474 lineation to < 5 m from contact surfaces.

475 - After paleomagnetic correction for rotation, the AMS data indicates that crustal
476 extension in Sabah at 7.9-7.3 Ma was oriented NW-SE at $319^\circ \pm 13.1^\circ$. This is
477 consistent with other evidence for Late Miocene extension in NW Borneo (Hall,
478 2013).

479 - In compressive settings, AMS foliations are consistent but lineations vary.
480 Likewise, in extensional settings, AMS lineations are consistent but foliations
481 vary. Consequently, compressional plutons can be distinguished by the relative
482 scales of the K1 and K3 confidence angles.

483 - A compilation of global AMS data for intrusions in extensional and
484 compressional regimes reveals the common occurrence of magnetic fabrics
485 preserving tectonic strain. This indicates that the AMS fabrics of plutonic rocks
486 have the potential to be employed globally to determine syn-magmatic tectonic
487 settings.

488

489 9. Acknowledgements

490 This study was funded by the Natural Environment Research Council. We thank
491 Carl Stevenson at the University of Birmingham for providing equipment and
492 training for our AMS analyses and discussion of our results. We wish to thank
493 Robert Hall, Mike Cottam and the SE Asia Research Group at Royal Holloway for
494 their support and discussions throughout this project. We thank Alim Biun, Felix
495 Tongkul and Maklarin Lakim for their assistance in facilitating the field season;
496 Jamili Nais of Sabah Parks who allowed us to work in the National Park; and the
497 mountain guides and researchers of Mt Kinabalu National Park, especially Alijen
498 “Jen”, Halli, Jasirin, Sokaibin, Maklarin Lakim, Sapinus, Samuel and Nicholas. We
499 thank Ian Alsop for his work as Editor in reviewing this paper, and an
500 Anonymous reviewer and František Hrouda and for taking the time to review
501 our submission. To receive such a positive review is greatly encouraging.

502 **10. References**

503

504 Aranguren, a., Cuevas, J., TubIa, J.M., RomAn-Berdiel, T., Casas-Sainz, A., Casas-
505 Ponsati, A., 2003. Granite laccolith emplacement in the Iberian arc: AMS and
506 gravity study of the La Tojiza pluton (NW Spain). *Journal of the Geological*
507 *Society* 160, 435–445. <https://doi.org/10.1144/0016-764902-079>

508 Arbaret, L., Diot, H., Bouchez, J.L., Lespinasse, P., de Saint-Blanquat, M., 1997.
509 Analogue 3D simple-shear experiments of magmatic biotite subfabrics.
510 *Granite: From Segregation of Melt to Emplacement Fabrics*. Springer, 129–
511 143.

512 Arbaret, L., Fernandez, A., Ježek, J., Ildefonse, B., Launeau, P., Diot, H., 2000.
513 Analogue and numerical modelling of shape fabrics: application to strain and
514 flow determination in magmas. *Geological Society of America Special Papers*
515 350, 97–109.

516 Archanjo, C.J., da Silva, E.R., Caby, R., 1999. Magnetic fabric and pluton
517 emplacement in a transpressive shear zone system: the Itaporanga porphyritic
518 granitic pluton (northeast Brazil). *Tectonophysics* 312, 331–345.

519 Archanjo, C.J., Olivier, P., Bouchez, J.L., 1992. Plutons granitiques du Seridó (NE du
520 Brésil): écoulement magmatique parallèle à la chaîne révélé par leur
521 anisotropie magnétique. *Bull. Sac. Géol. France* 163, 509–520.

522 Archanjo, C.J., Trindade, R.I., Bouchez, J.L., Ernesto, M., 2002. Granite fabrics and
523 regional-scale strain partitioning in the Seridó belt (Borborema Province, NE
524 Brazil). *Tectonics* 21, 1003.

525 Benn, K., 2010. Anisotropy of magnetic susceptibility fabrics in syntectonic plutons
526 as tectonic strain markers: the example of the Canso pluton, Meguma Terrane,
527 Nova Scotia. *Earth and Environmental Science Transactions of the Royal*
528 *Society of Edinburgh* 100, 147–158.
529 <https://doi.org/10.1017/S1755691009016028>

530 Benn, K., Paterson, S.R., Lund, S.P., Pignotta, G.S., Kruse, S., 2001. Magmatic
531 fabrics in batholiths as markers of regional strains and plate kinematics:
532 example of the Cretaceous Mt. Stuart batholith. *Physics and Chemistry of the*
533 *Earth, Part A: Solid Earth and Geodesy* 26, 343–354.
534 [https://doi.org/10.1016/S1464-1895\(01\)00064-3](https://doi.org/10.1016/S1464-1895(01)00064-3)

535 Blumenfeld, P., Bouchez, J.-L., 1988. Shear criteria in granite and migmatite
536 deformed in the magmatic and solid states. *Journal of Structural Geology* 10,
537 361–372. [https://doi.org/10.1016/0191-8141\(88\)90014-4](https://doi.org/10.1016/0191-8141(88)90014-4)

538 Bouchez, J.L., 1997. Granite is never isotropic: an introduction to AMS studies of
539 granitic rocks. *Granite: From Segregation of Melt to Emplacement Fabrics*.
540 Springer, 95–112.

541 Bouillin, J.-P., Bouchez, J.-L., Lespinasse, P., Pe^cher, a., 1993. Granite
542 emplacement in an extensional setting: an AMS study of the magmatic
543 structures of Monte Capanne (Elba, Italy). *Earth and Planetary Science Letters*
544 118, 263–279. [https://doi.org/10.1016/0012-821X\(93\)90172-6](https://doi.org/10.1016/0012-821X(93)90172-6)

545 Bucher, K., Grapes, R., 2011. *Petrogenesis of metamorphic rocks*, 8th Edition. ed.
546 Springer, Heidelberg, Germany.

547 Burton-Johnson, A., Macpherson, C.G., Hall, R., 2017. Internal structure and
548 emplacement mechanism of composite plutons: evidence from Mt Kinabalu,
549 Borneo. *Journal of the Geological Society* 174, 180–191.

- 550 Burton-Johnson, A., Macpherson, C.G., Ottley, C.J., Nowell, G.M., Boyce, A.J., in
551 review. Generation of Mt Kinabalu granite by crustal contamination of
552 intraplate magma modelled by Equilibrated Major Element Assimilation with
553 Fractional Crystallisation (EME-AFC). *Journal of Petrology*.
- 554 Collenette, P., 1965. The geology and mineral resources of the Pensiangan and Upper
555 Kinabatangan area, Sabah. Malaysia Geological Survey Borneo Region,
556 Memoir 12 150.
- 557 Cottam, M.A., Hall, R., Sperber, C., Armstrong, R., 2010. Pulsed emplacement of the
558 Mount Kinabalu granite, northern Borneo. *Journal of the Geological Society*
559 167, 49–60. <https://doi.org/10.1144/0016-76492009-028>. Pulsed
- 560 Cottam, M.A., Hall, R., Sperber, C., Kohn, B.P., Forster, M.A., Batt, G.E., 2013.
561 Neogene rock uplift and erosion in northern Borneo: evidence from the
562 Kinabalu granite, Mount Kinabalu. *Journal of the Geological Society* 170,
563 805–816. <https://doi.org/10.1144/jgs2011-130>
- 564 Cruden, A.R., 1999. Magnetic fabric evidence for conduit-fed emplacement of a
565 tabular intrusion: Dinkey Creek Pluton, central Sierra Nevada batholith,
566 California. *Journal of Geophysical Research: Solid Earth* 104, 511–530.
- 567 Davis, J.C., 1986. *Statistics and data analysis in geology*, 2nd Edition. ed. Wiley &
568 Sons, New York.
- 569 de Saint Blanquat, M., Tikoff, B., 1997. Development of magmatic to solid-state
570 fabrics during syntectonic emplacement of the Mono Creek Granite, Sierra
571 Nevada Batholith. *Granite: From Segregation of Melt to Emplacement*
572 *Fabrics*. Springer, 231–252.
- 573 Deng, X., Wu, K., Yang, K., 2013. Emplacement and deformation of Shigujian
574 syntectonic granite in central part of the Dabie orogen: Implications for
575 tectonic regime transformation. *Science China Earth Sciences* 56, 980–992.
- 576 Dhonau, T.J., Hutchison, C.S., 1965. The Darvel Bay area, East Sabah, Malaysia.
577 Malaysia Geological Survey Borneo Region, Annual Report for 1965 141–
578 160.
- 579 Ernst, R.E., Baragar, W.R.A., 1992. Evidence from magnetic fabric for the flow
580 pattern of magma in the Mackenzie giant radiating dyke swarm. *Nature* 356,
581 511.
- 582 Fuller, M., Haston, R., Lin, J., Richter, B., 1991. Tertiary paleomagnetism of regions
583 around the South China Sea. *Journal of Southeast ...* 6, 161–184.
- 584 Gay, N. C., 1968. The motion of rigid particles embedded in a viscous fluid during
585 pure shear deformation of the fluid. *Tectonophysics* 5, 81–88.
- 586 Gay, No C., 1968. Pure shear and simple shear deformation of inhomogeneous
587 viscous fluids. 1. Theory. *Tectonophysics* 5, 211–234.
- 588 Gleizes, G., Leblanc, D., Olivier, P., Bouchez, J., 2001. Strain partitioning in a pluton
589 during emplacement in transpressional regime: the example of the Néouvielle
590 granite (Pyrenees). *International Journal of Earth Sciences* 90, 325–340.
- 591 Grove, C., Jerram, D.A., 2011. jPOR: An ImageJ macro to quantify total optical
592 porosity from blue-stained thin sections. *Computers & Geosciences* 37, 1850–
593 1859.
- 594 Gutiérrez, F., Payacán, I., Gelman, S.E., Bachmann, O., Parada, M. a., 2013. Late-
595 stage magma flow in a shallow felsic reservoir: Merging the anisotropy of
596 magnetic susceptibility record with numerical simulations in La Gloria Pluton,
597 central Chile. *Journal of Geophysical Research: Solid Earth* 118, 1984–1998.
598 <https://doi.org/10.1002/jgrb.50164>

- 599 Hall, R., 2013. Contraction and extension in northern Borneo driven by subduction
600 rollback. *Journal of Asian Earth Sciences* 76, 399–411.
601 <https://doi.org/10.1016/j.jseaes.2013.04.010>
- 602 Harrison, R.J., Muraszko, J., Heslop, D., Lascu, I., Muxworthy, A.R., Roberts, A.P.,
603 2018. An Improved Algorithm For Unmixing First-Order Reversal Curve
604 Diagrams Using Principal Component Analysis. *Geochemistry, Geophysics,*
605 *Geosystems*.
- 606 Hrouda, F., Faryad, S.W., 2017. Magnetic fabric overprints in multi-deformed
607 polymetamorphic rocks of the Gemeric Unit (Western Carpathians) and its
608 tectonic implications. *Tectonophysics* 717, 83–98.
- 609 Hrouda, F., Jacko, S., Hanák, J., 1988. Parallel magnetic fabrics in metamorphic,
610 granitoid and sedimentary rocks of the Branisko and Čierna Hora Mountains
611 (E Slovakia) and their tectonometamorphic control. *Physics of the Earth and*
612 *Planetary Interiors* 51, 271–289.
- 613 Hrouda, F., Ježek, J., 2017. Role of single-domain magnetic particles in creation of
614 inverse magnetic fabrics in volcanic rocks: A mathematical model study.
615 *Studia Geophysica et Geodaetica* 61, 145–161.
- 616 Hunt, C.P., Moskowitz, B.M., Banerjee, S.K., 1995. Magnetic properties of rocks and
617 minerals. In: Ahrens, T.J. (Ed.), *Rock Physics & Phase Relations: A*
618 *Handbook of Physical Constants*. AGU, Washington D.C., 189–204.
- 619 Hutchison, C., 2000. A Miocene collisional belt in north Borneo: uplift mechanism
620 and isostatic adjustment quantified by thermochronology. *Journal of the*
621 *Geological Society* 157, 783–793.
- 622 Hutchison, C.S., 1996. The “Rajang accretionary prism” and “Lupar Line” problem of
623 Borneo. *Geological Society, London, Special Publications* 106, 247–261.
624 <https://doi.org/10.1144/GSL.SP.1996.106.01.16>
- 625 Hutton, D.H., 1988. Granite emplacement mechanisms and tectonic controls:
626 inferences from deformation studies. *Earth and Environmental Science*
627 *Transactions of the Royal Society of Edinburgh* 79, 245–255.
- 628 Jacobson, G., 1970. Gunung Kinabalu Area, Sabah, Malaysia. *Geological Survey*
629 *Malaysia, Kuching, Sarawak*.
- 630 Jeffery, G.B., 1922. The motion of ellipsoidal particles immersed in a viscous fluid.
631 *Proc. R. Soc. Lond. A* 102, 161–179.
- 632 Ježek, J., Hrouda, F., 2004. Determination of the orientation of magnetic minerals
633 from the anisotropy of magnetic susceptibility. *Geological Society, London,*
634 *Special Publications* 238, 9–20.
- 635 King, R.C., Backé, G., Morley, C.K., Hillis, R.R., Tingay, M.R.P., 2010. Balancing
636 deformation in NW Borneo: Quantifying plate-scale vs. gravitational tectonics
637 in a delta and deepwater fold-thrust belt system. *Marine and Petroleum*
638 *Geology* 27, 238–246. <https://doi.org/10.1016/j.marpetgeo.2009.07.008>
- 639 Kirk, H.J.C., 1968. The igneous rocks of Sarawak and Sabah. *Geological Survey*
640 *Borneo Region, Malaysia, Bulletin* 5, 201.
- 641 Koopmans, B.N., 1967. Deformation of the metamorphic rocks and the Chert–Spilite
642 Formation in the southern part of the Darvel Bay area, Sabah. *Geological*
643 *Survey of Malaysia, Borneo Region, Bulletin* 8, 14–24.
- 644 Lennox, P.G., de Wall, H., Durney, D.W., 2016. Correlation between magnetic
645 fabrics, strain and biotite microstructure with increasing mylonitisation in the
646 pre-tectonic Wyangala Granite, Australia. *Tectonophysics* 676, 170–197.

- 647 Leong, K.M., 1974. The geology and mineral resources of the Upper Segama Valley
648 and Darvel Bay area, Sabah, Malaysia. Geological Survey of Malaysia,
649 Memoir 4.
- 650 Lin, W., Charles, N., Chen, Y., Chen, K., Faure, M., Wu, L., Wang, F., Li, Q., Wang,
651 J., Wang, Q., 2013. Late Mesozoic compressional to extensional tectonics in
652 the Yiwulüshan massif, NE China and their bearing on the Yinshan–Yanshan
653 orogenic belt: part II: anisotropy of magnetic susceptibility and gravity
654 modeling. *Gondwana Research* 23, 78–94.
- 655 Martins, H.C., Sant’Ovaia, H., Abreu, J., Oliveira, M., Noronha, F., 2011.
656 Emplacement of the Lavadores granite (NW Portugal): U/Pb and AMS results.
657 *Comptes Rendus Geoscience* 343, 387–396.
- 658 Olivier, P., de Saint Blanquat, M., Gleizes, G., Leblanc, D., 1997. Homogeneity of
659 granite fabrics at the metre and dekametre scales. *Granite: From Segregation
660 of Melt to Emplacement Fabrics*. Springer, 113–127.
- 661 Orlický, O., 1990. Detection of magnetic carriers in rocks: results of susceptibility
662 changes in powdered rock samples induced by temperature. *Physics of the
663 Earth and Planetary Interiors* 63, 66–70.
- 664 Otoh, S., Jwa, Y.-J., Nomura, R., Sakai, H., 1999. A preliminary AMS (anisotropy of
665 magnetic susceptibility) study of the Namwon granite, southwest Korea.
666 *Geosciences Journal* 3, 31–41.
- 667 Owens, W.H., 1994. Laboratory drilling of field-orientated block samples. *Journal of
668 Structural Geology* 16, 1719–1721. [https://doi.org/10.1016/0191-
669 8141\(94\)90137-6](https://doi.org/10.1016/0191-8141(94)90137-6)
- 670 Park, J.K., Tanczyk, E.I., Desbarats, A., 1988. Magnetic fabric and its significance in
671 the 1400 Ma Mealy diabase dykes of Labrador, Canada. *Journal of
672 Geophysical Research: Solid Earth* 93, 13689–13704.
- 673 Paterson, S.R., Fowler, T.K., Schmidt, K.L., Yoshinobu, A.S., Yuan, E.S., Miller,
674 R.B., 1998. Interpreting magmatic fabric patterns in plutons. *Lithos* 44, 53–82.
675 [https://doi.org/10.1016/S0024-4937\(98\)00022-X](https://doi.org/10.1016/S0024-4937(98)00022-X)
- 676 Paterson, S.R., Tobisch, O.T., 1988. Using pluton ages to date regional deformations:
677 problems with commonly used criteria. *Geology* 16, 1108–1111.
- 678 Petronis, M.S., O’Driscoll, B., 2013. Emplacement of the early Miocene Pinto Peak
679 intrusion, Southwest Utah, USA. *Geochemistry, Geophysics, Geosystems* 14,
680 5128–5145.
- 681 Petronis, M.S., O’Driscoll, B., Stevenson, C.T.E., Reavy, R.J., 2012. Controls on
682 emplacement of the Caledonian Ross of Mull Granite, NW Scotland:
683 Anisotropy of magnetic susceptibility and magmatic and regional structures.
684 *Geological Society of America Bulletin* 124, 906–927.
685 <https://doi.org/10.1130/B30362.1>
- 686 Pitcher, W.S., 1997. The nature and origin of granite, Second Edition. ed. Chapman &
687 Hall, London, UK.
- 688 Pubellier, M., Morley, C.K., 2013. The Basins of Sundaland (SE Asia); evolution and
689 boundary conditions. *Marine and Petroleum Geology* 58, 555–578.
- 690 Reinhard, M., Wenk, E., 1951. Geology of the Colony of North Borneo. *British
691 Borneo Geological Survey Bulletin* 1.
- 692 Sadeghian, M., Bouchez, J.L., Nédélec, a., Siqueira, R., Valizadeh, M.V., 2005. The
693 granite pluton of Zahedan (SE Iran): a petrological and magnetic fabric study
694 of a syntectonic sill emplaced in a transtensional setting. *Journal of Asian
695 Earth Sciences* 25, 301–327. <https://doi.org/10.1016/j.jseaes.2004.03.001>

- 696 Schofield, D.I., D'Lemos, R.S., 1998. Relationships between syn-tectonic granite
697 fabrics and regional PTtd paths: an example from the Gander-Avalon
698 boundary of NE Newfoundland. *Journal of Structural Geology* 20, 459–471.
- 699 Schulmann, K., Ježek, J., 2012. Some remarks on fabric overprints and constrictional
700 AMS fabrics in igneous rocks. *International Journal of Earth Sciences* 101,
701 705–714.
- 702 Schulmann, K., Ježek, J., Venera, Z., 1997. Perpendicular linear fabrics in granite:
703 markers of combined simple shear and pure shear flows? *Granite: From*
704 *Segregation of Melt to Emplacement Fabrics*. Springer, 159–176.
- 705 Stephenson, A., Sadikun, S. t, Potter, D.K., 1986. A theoretical and experimental
706 comparison of the anisotropies of magnetic susceptibility and remanence in
707 rocks and minerals. *Geophysical Journal International* 84, 185–200.
- 708 Swauger, D.A., Hutchison, C.S., Bergman, S.C., Graves, J.E., 2000. Age and
709 emplacement of the Mount Kinabalu pluton. *Geological Society of Malaysia*
710 *Bulletin* 44, 159–163.
- 711 Talbot, J.-Y., Chen, Y., Faure, M., 2005. A magnetic fabric study of the Aigoual–
712 Saint Guiral–Liron granite pluton (French Massif Central) and relationships
713 with its associated dikes. *Journal of Geophysical Research* 110, B12106–
714 B12106. <https://doi.org/10.1029/2005JB003699>
- 715 Tikoff, B., Davis, M.R., Teyssier, C., Blanquat, M. de S., Habert, G., Morgan, S.,
716 2005. Fabric studies within the Cascade Lake shear zone, Sierra Nevada,
717 California. *Tectonophysics* 400, 209–226.
- 718 Tomek, F., Žák, J., Verner, K., Holub, F.V., Sláma, J., Paterson, S.R., Memeti, V.,
719 2017. Mineral fabrics in high-level intrusions recording crustal strain and
720 volcano–tectonic interactions: the Shellenbarger pluton, Sierra Nevada,
721 California. *Journal of the Geological Society* 174, 193–208.
- 722 Tomek, F., Žák, J., Verner, K., Holub, F.V., Sláma, J., Paterson, S.R., Memeti, V.,
723 2016. Mineral fabrics in high-level intrusions recording crustal strain and
724 volcano–tectonic interactions: the Shellenbarger pluton, Sierra Nevada,
725 California. *Journal of the Geological Society* jgs2015-151.
726 <https://doi.org/10.1144/jgs2015-151>
- 727 van Hattum, M.W., Hall, R., Pickard, A.L., Nichols, G.J., 2006. Southeast Asian
728 sediments not from Asia: Provenance and geochronology of north Borneo
729 sandstones. *Geology* 34, 589–592.
- 730 Vignerresse, J.-L., 1999. Should felsic magmas be considered as tectonic objects, just
731 like faults or folds? *Journal of Structural Geology* 21, 1125–1130.
- 732 Vogt, E., Flower, M., 1989. Genesis of the Kinabalu (Sabah) granitoid at a
733 subduction-collision junction. *Contributions to Mineralogy and Petrology*
734 493–509.
- 735 Walz, F., 2002. The Verwey transition-a topical review. *Journal of Physics:*
736 *Condensed Matter* 14, R285.
- 737 Whitney, D.L., Evans, B.W., 2010. Abbreviations for names of rock-forming
738 minerals. *American Mineralogist* 95, 185.
- 739 Wilson, J., 1998. Magnetic susceptibility patterns in a Cordilleran granitoid: the Las
740 Tazas complex, northern Chile. *Journal of Geophysical Research: Solid Earth*
741 103, 5257–5267.
- 742

743 **Figure Captions**

744 Fig. 1. Relationship of mineral fabrics (foliation and lineation) and the principal
745 vectors of magnetic susceptibility describing the AMS fabric (K1 – Maximum
746 susceptibility; K2 – Intermediate susceptibility; K3 – Minimum susceptibility) to
747 the strain ellipsoid and the principal stress directions during crystallisation (σ_1 –
748 Maximum compression direction; σ_2 – Intermediate compression direction; σ_3 –
749 Minimum compression direction).

750

751 Fig. 2. Example stereonet (lower hemisphere projection) of the resultant AMS
752 fabrics developed in response to coaxial and non-coaxial strain. Shown are the
753 principal stress directions, simple shear direction, and principal vectors of
754 magnetic susceptibility: K1 – Maximum susceptibility; K2 – Intermediate
755 susceptibility; K3 – Minimum susceptibility.

756

757 Fig. 3. A) Regional geography of Mt Kinabalu and Sabah within SE Asia. B) Aerial
758 photograph of Mt Kinabalu from the south highlighting its extreme vertical relief;
759 courtesy of Tony Barber. C) Internal structure and emplacement ages (Cottam et
760 al., 2010) of the Mt Kinabalu intrusion, as determined from field evidence
761 (Burton-Johnson et al., 2017).

762

763 Fig. 4. Representative thin section images of (a) the Alexandra
764 Tonalite/Granodiorite, and (b) the King Granite (itself representative of the post-
765 Alexandra units). Rose diagrams show the orientations hornblende and biotite
766 crystals in each section. Sections are arbitrarily orientated. Abbreviations as in
767 Fig. 1, plus Hb – Hornblende; Bt – Biotite.

768

769 Fig. 5. Geological map of Mt Kinabalu highlighting the (A) foliation and (B)
770 lineation of the summit plateaux and eastern ridge. Variations in these
771 orientations close to the contact between the King Granite and Paka Porphyritic
772 Granite (box shown in B) are shown in (C) and (D). Abbreviations as in Fig. 5.

773

774 Fig. 6. Relationship of the degree of magnetic anisotropy, P' , to the mean bulk
775 susceptibility, K_{Mean} (A), and shape parameter of the AMS fabric, T (B).
776 Abbreviations: Tn – Tonalite, Gd – Granodiorite, Gt – Granite, Pph – Porphyritic
777 Granite.

778

779 Fig. 7. Variation in bulk magnetic susceptibility of each granitic unit with
780 temperature. Abbreviations as in Fig. 5.

781

782 Fig. 8. Hysteresis loops and First Order Reversal curves for: a) the Alexandra
783 Tonalite/Granodiorite; b) the King Granite. The King Granite is representative of
784 the plutons' other composite units. Two synthetic binary mixtures of c) purely
785 multi-domain (MD), and d) a mixture of multi- and single-domain (SD) magnetite
786 are shown for comparison (Harrison et al., 2018).

787

788 Fig. 9. Lower hemisphere projections of the lineation (K1) and pole to the
789 foliation (K3) for the AMS fabric of each of Mt Kinabalu's composite units.
790 Abbreviations as in Fig. 5.

791

792 Fig. 10. Poles to planes for faults, aplite dykes and mafic dykes cross-cutting Mt
793 Kinabalu (Burton-Johnson et al., 2017) compared to lineation (K1) and poles to
794 foliation (K3) of the AMS fabric (excluding the Donkey Granite and Mesilau
795 Porphyritic Granite). Open arrows illustrate the interpreted associated principal
796 stress directions for structural data. Diamonds indicate maximum eigenvectors.

797

798 Fig. 11. Global compilation of lineation (K1) and pole to foliation (K3) directions
799 of AMS data from intrusions emplaced in both extensional and compressive
800 tectonic settings showing the orientation of the principal extensional or
801 compressional direction generating the tectonic fabric.

802 Mt Kinabalu, Borneo – This study; Yiwulüshan massif - Lin et al. (2013);
803 Zahedian - Sadeghian et al. (2005); Monte Capanne - Bouillin et al. (1993);
804 Aigoual–Saint Guiral–Liron - Talbot et al. (2005); La Tojiza - Aranguren et al.
805 (2003); Shigujian - Deng et al. (2013); Ross of Mull - Petronis et al. (2012); Pinto
806 Peak - Petronis and O’Driscoll (2013); Namwon - Otoh et al. (1999); Lavadores -
807 Martins et al. (2011); Las Tazes - Wilson (1998); Wyangala - Lennox et al.
808 (2016); La Gloria - Gutiérrez et al. (2013); Mt Stuart - Benn et al. (2001); Dinky
809 Creek - Cruden (1999); Shellenbarger - Tomek et al. (2017); Mono Creek - de
810 Saint Blanquat and Tikoff (1997).

811

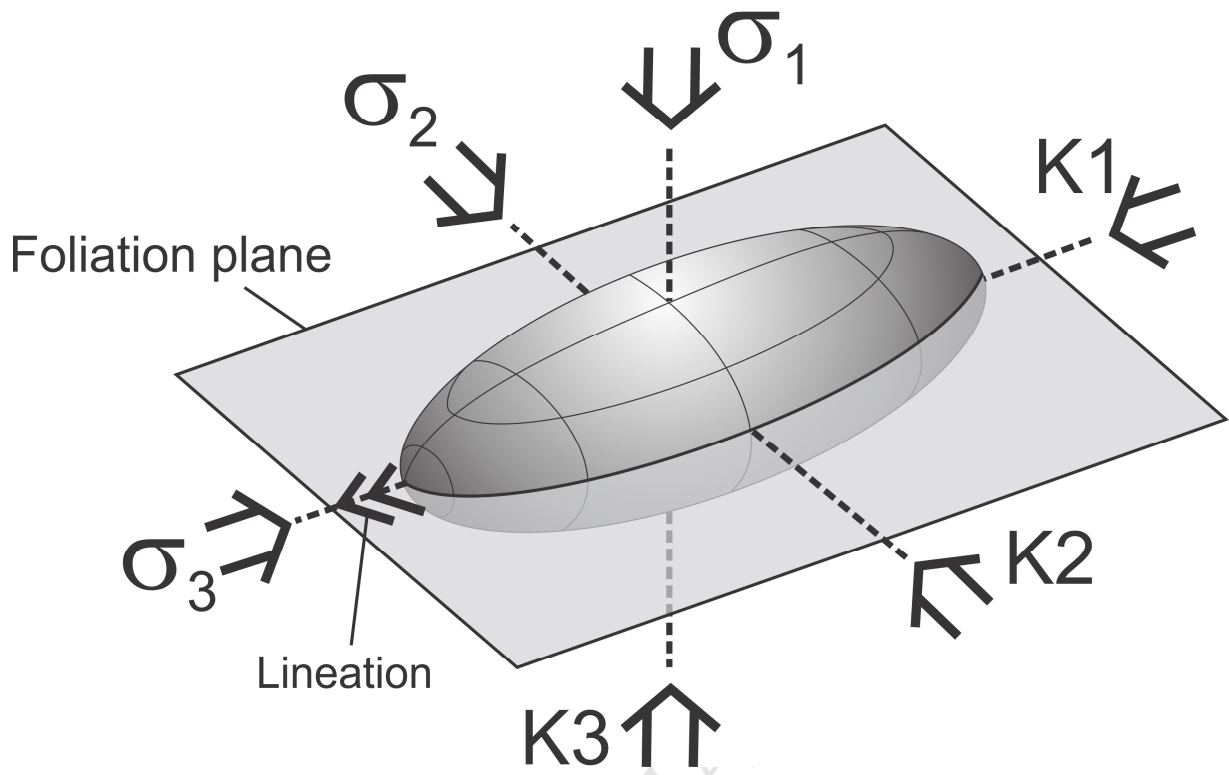
812 Fig. 12. 95% symmetrical confidence limits of the mean spherical K1 and K3
813 vector for the compressional and extensional plutons in Fig. 11. Compressional
814 plutons can be identified at 90% confidence where “K1 95% Confidence Angle /
815 K3 95% Confidence Angle” <1.2, and extensional plutons can be identified at
816 90% confidence where “K1 95% Confidence Angle / K3 95% Confidence Angle”
817 >1.5.

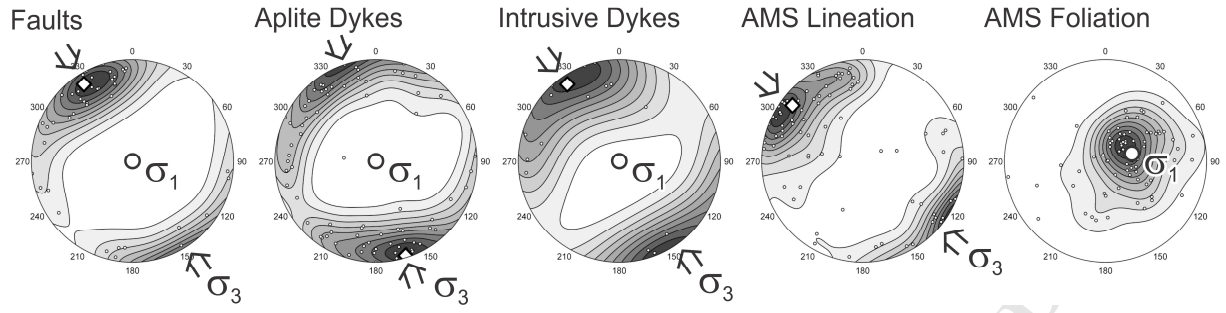
818

819 Table 1. Summary of U-Pb zircon ages (Cottam et al., 2010), SiO₂ and Mg#
820 (Burton-Johnson et al., in review), estimated volumes and modal mineralogies
821 (Burton-Johnson et al., 2017) of the major granitoid units. Abbreviations used:
822 Tn – Tonalite; Gd – Granodiorite; Gt – Granite; Pph – Porphyritic Granite; Qz –
823 Quartz; Pl – Plagioclase; Kfs – Potassium Feldspar; Hb – Hornblende; Bt – Biotite;
824 Cpx. – Clinopyroxene; Ap – Apatite; Ep – Epidote; Zrn – Zircon; Spn – Sphene
825 (Whitney and Evans, 2010).

Unit	Alexandra Tn/Gd	Low's Gt	King Gt	Donkey Gt	Paka Pph	Mesilau Pph
U-Pb Age (Ma)	7.85 ±0.08	7.69 ±0.07 - 7.64 ±0.11	7.46 ±0.08 - 7.44 ±0.09	7.46 > t > 7.32	7.32 ±0.09 - 7.22 ±0.07	-
Approx. Vol. (Km ³)	0.2	2 (W) 4 (N)	90	0.4	40	40
SiO ₂ (wt. %)	61-65	59-64	62-66	63-65	63-67	60-65
Mg#	47-52	50-53	44-53	43-50	44-47	44-47
Phases (Modal %)						
Qz	23-28	16-28	14-27	23	15-21	7-21
Pl	40-45	25-33	21-38	26	23-33	24-28
Kfs	4-7	18-29	26-36	25	23-35	38-48
Hb	4-13	21-28	9-21	11	11-24	8-23
Bt	9-19	4-7	0-5	13	1-2	0-5
Cpx	-	-	-	-	-	0-2
Accessory	Ap, Ep	Ap, Ep, Zrn	Ap, Ep, Zrn	Ap	Ap	Ap, Spn

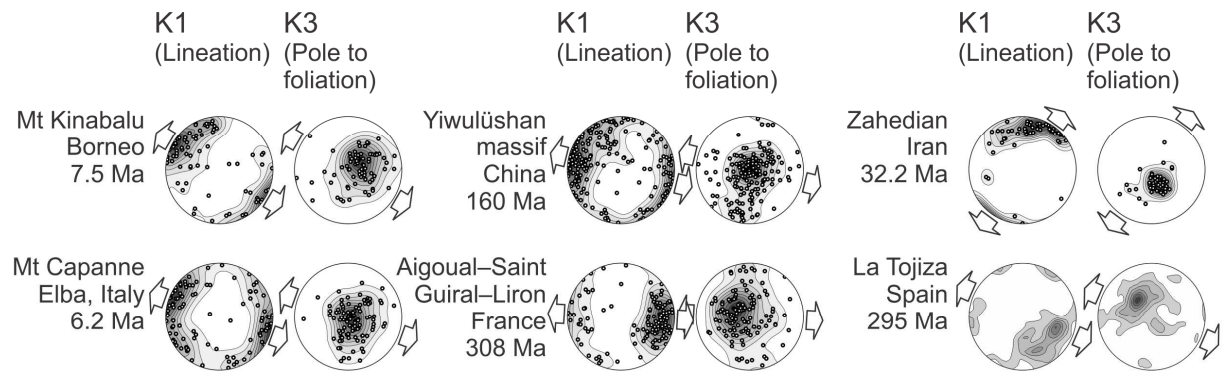
Table 1. Summary of U-Pb zircon ages (Cottam et al., 2010), SiO₂ and Mg# (Burton-Johnson et al., In Review), estimated volumes and modal mineralogies (Burton-Johnson et al., 2017) of the major granitoid units. Abbreviations used: Tn – Tonalite; Gd – Granodiorite; Gt – Granite; Pph – Porphyritic Granite; Qz – Quartz; Pl – Plagioclase; Kfs – Potassium Feldspar; Hb – Hornblende; Bt – Biotite; Cpx. – Clinopyroxene; Ap – Apatite; Ep – Epidote; Zrn – Zircon; Spn – Sphene (Whitney and Evans, 2010).



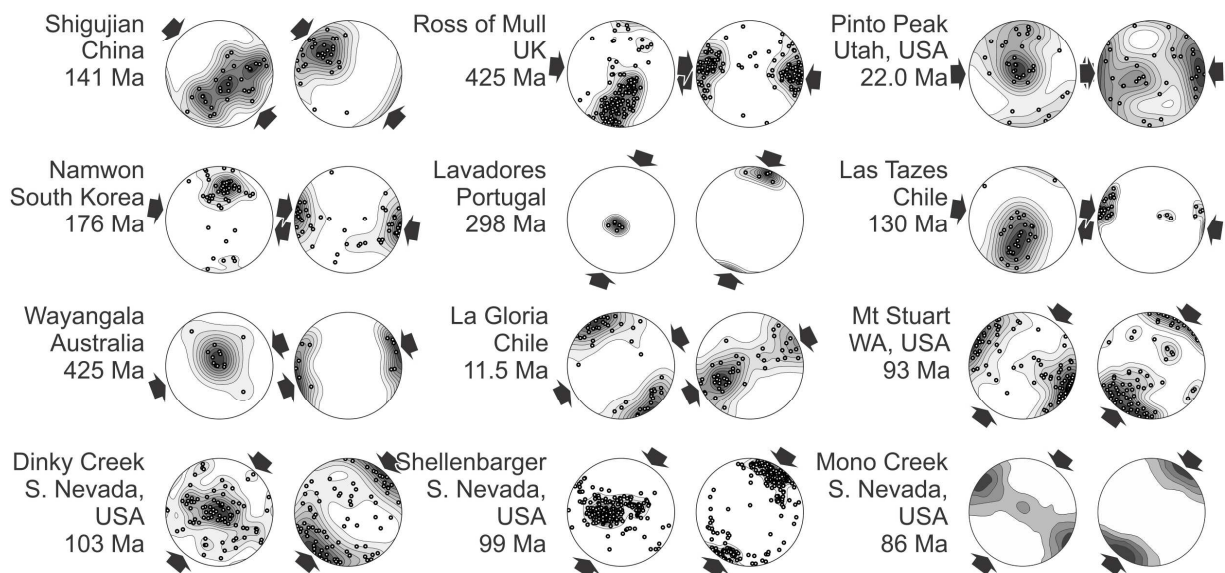


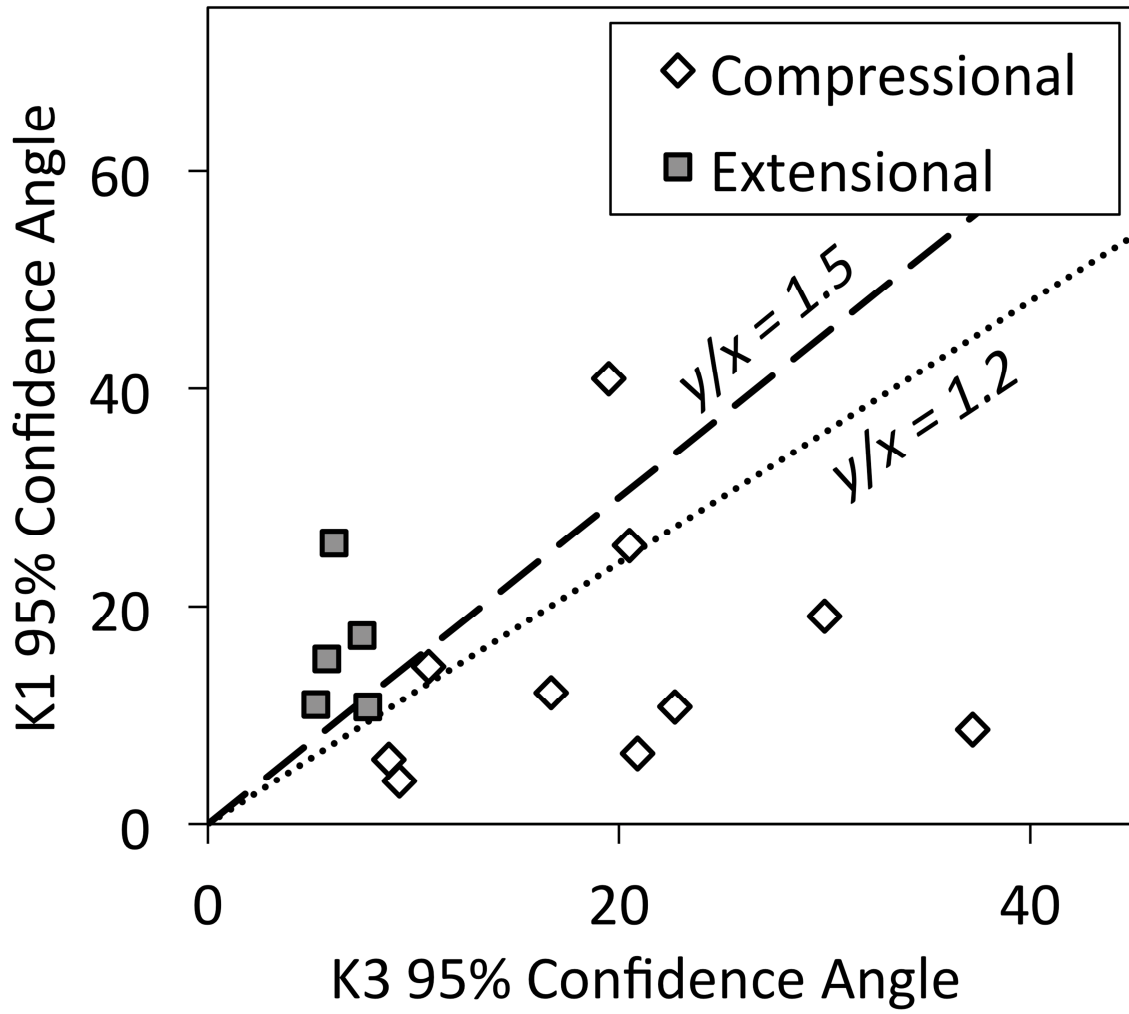
ACCEPTED MANUSCRIPT

Extensional Plutons

Extension direction: 

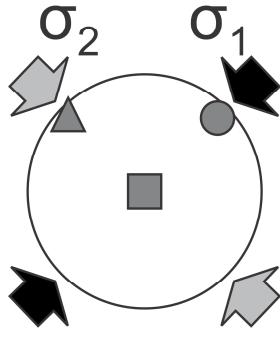
Compressional Plutons

Compression direction: 



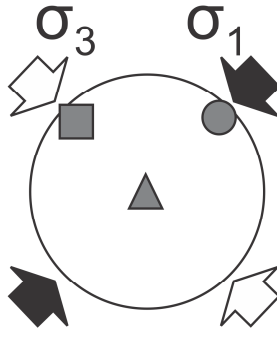
Coaxial Pure Shear

High lateral
compression
(σ_3 vertical)



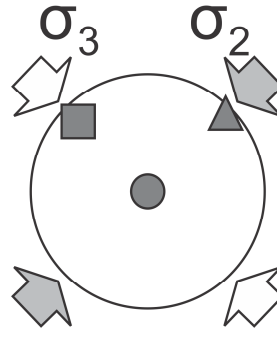
a)

Moderate lateral
compression
(σ_2 vertical)



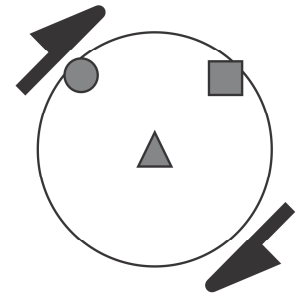
b)

Extensional
(σ_1 vertical)



c)

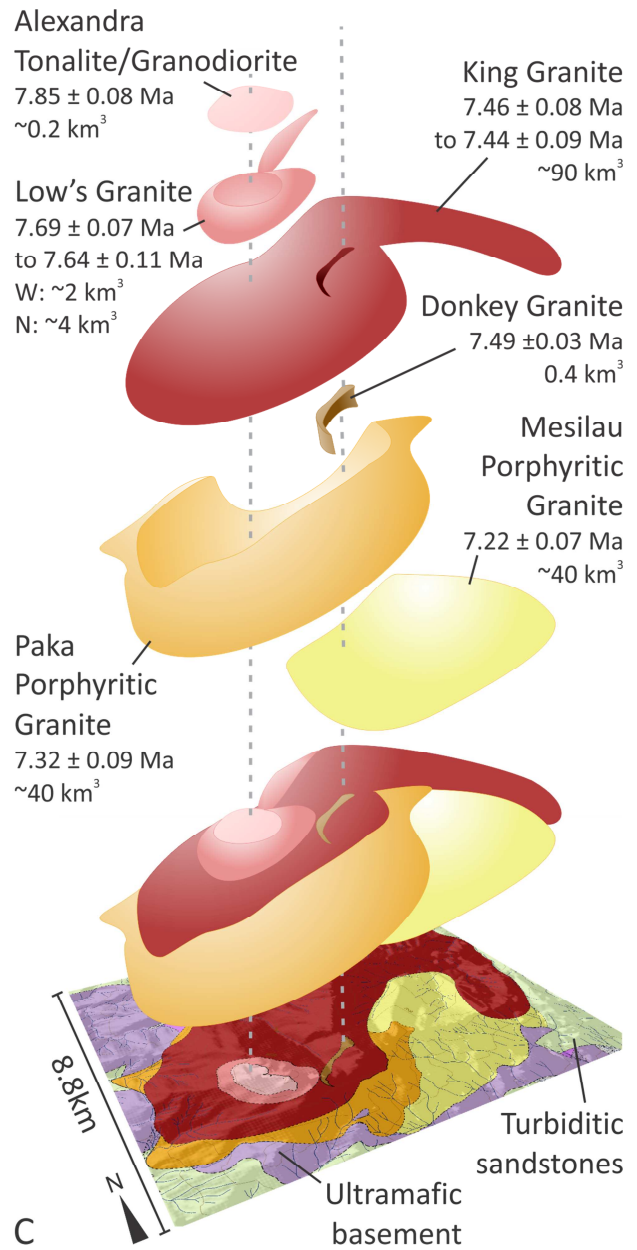
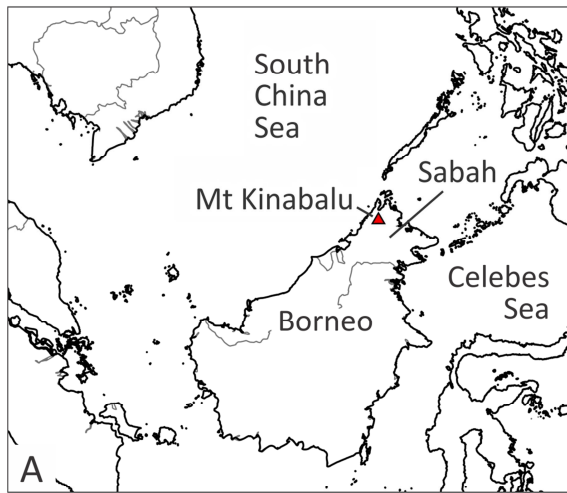
Non-Coaxial Simple Shear



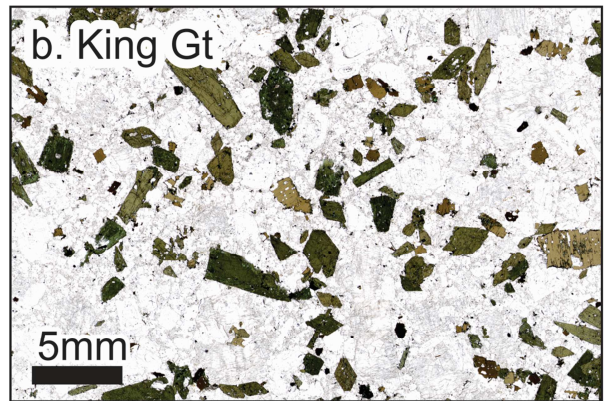
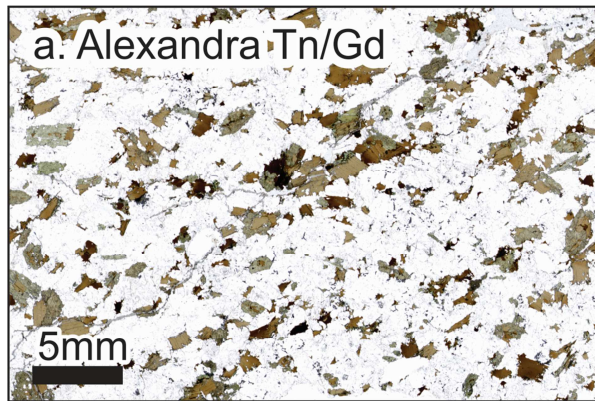
d)

AMS Axes: ■ K1 ▲ K2 ● K3

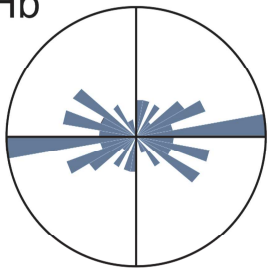
ACCEPTED MANUSCRIPT



ACC

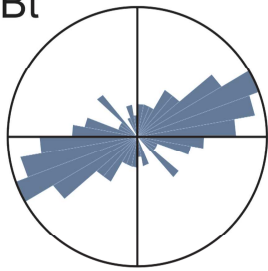


Hb



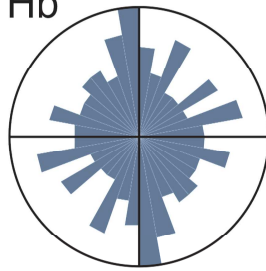
n = 39

Bt



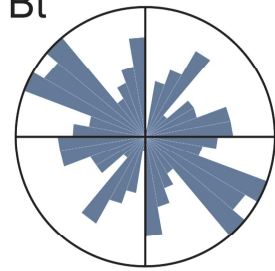
n = 87

Hb



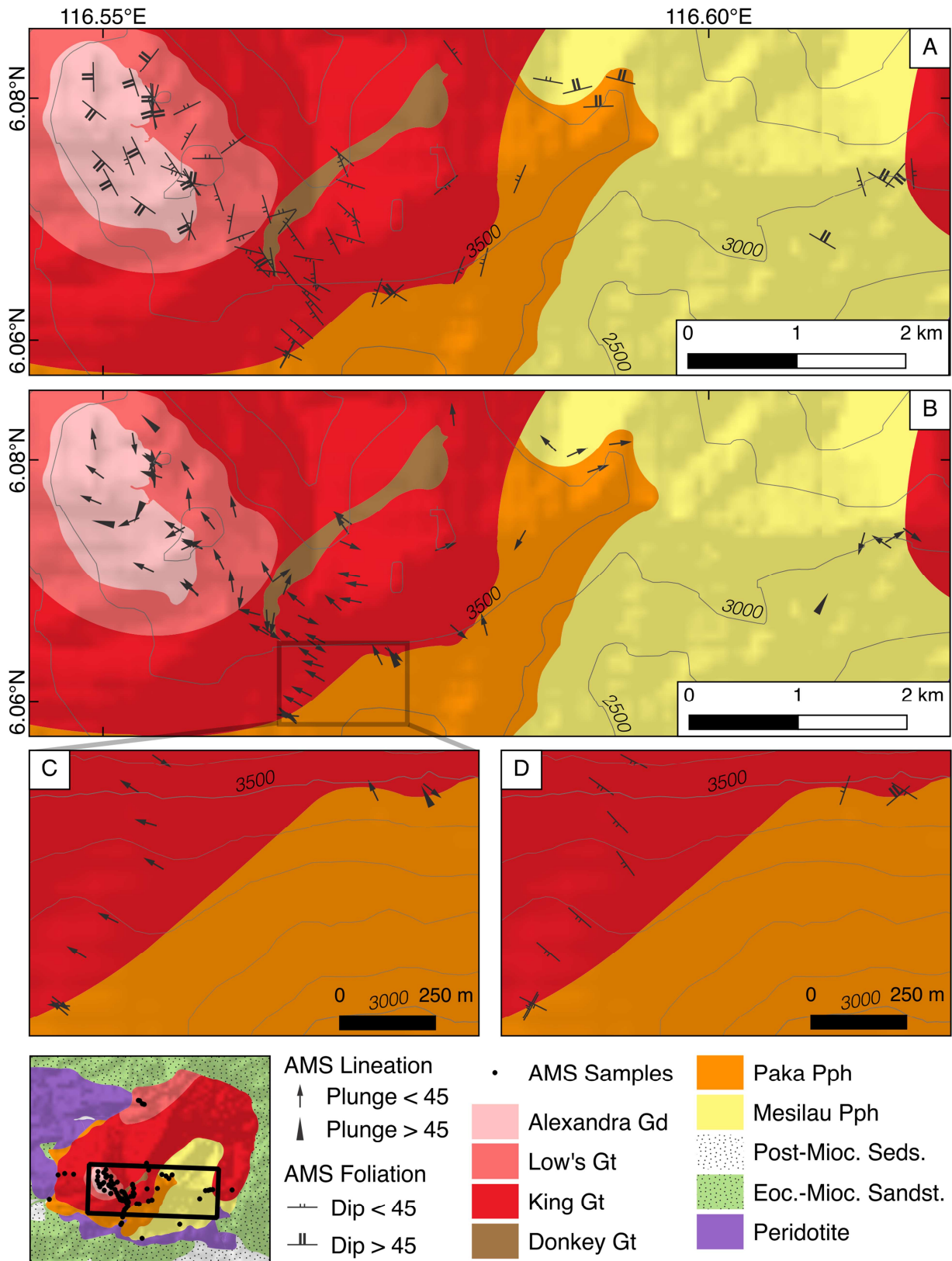
n = 109

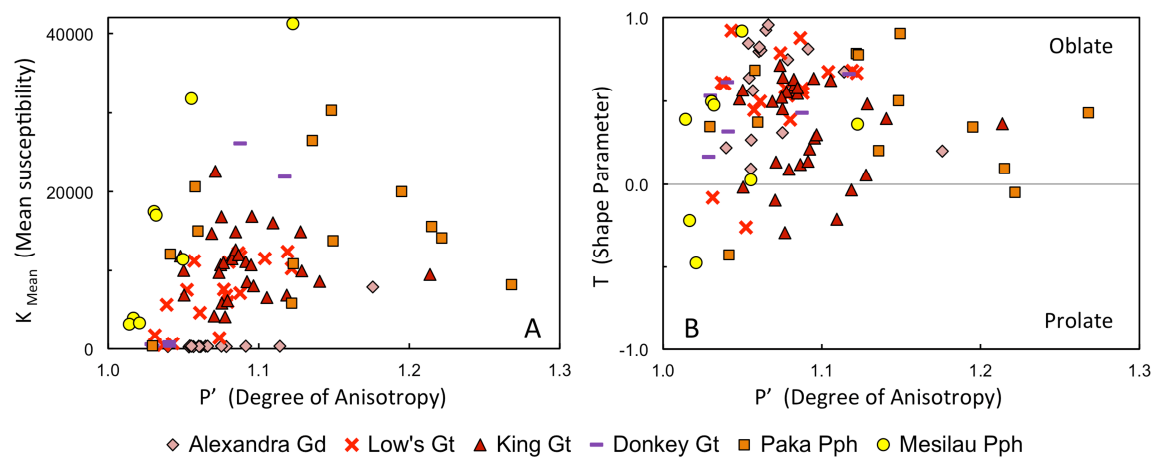
Bt



n = 93

ACCEPTED MANUSCRIPT





ACCEPTED

